

# Investigations of the emission geometry of the four-component radio pulsar J0631+1036

Mateus M. Teixeira<sup>1</sup>, Joanna M. Rankin<sup>1,3</sup>, Geoffrey A.E. Wright<sup>2,3</sup> & J. Dyks<sup>4</sup>

<sup>1</sup>*Department of Physics, University of Vermont, Burlington, VT 05405\**

<sup>2</sup>*Astronomy Centre, University of Sussex, Falmer, BN1 9QJ, UK†*

<sup>3</sup>*Astronomical Institute “Anton Pannekoek”, University of Amsterdam, Science Park 904, 1098 XH Amsterdam, The Netherlands*

<sup>4</sup>*Nicolaus Copernicus Astronomical Center, Radańska 8, 87-100, Toruń, Poland‡*

Originally drafted 2011 09 22

## ABSTRACT

Radio pulsar J0631+1036 presents a remarkably clear example of a rare four-component profile, and with apparently large aberration/retardation indicated by its linear polarization-angle traverse, but on closer study its profiles are difficult to understand and interpret. Given the broad success of the core/double-cone geometric model in describing the profiles of slower pulsars, we assess whether it could be appropriate for J0631+1036. The emission geometry resulting from application of this model is not implausible; however, it is difficult to reconcile it with the well resolved forms of the inner component pair. Overall, we are forced to conclude that this pulsar emits somewhat differently than its closest peers, perhaps because it is located within a dense star-forming region. Both a bi-directional emission model and a “wedge” model are discussed as alternatives.

**Key words:** miscellaneous – aberration/retardation – emission height – emission geometry – methods: – data analysis – pulsars: general, individual (J0631+1036)

## I. INTRODUCTION

The very unusual pulse profile of pulsar J0631+1036 in Figure 1 (top) consists of two pairs of nearly symmetrical components, all highly linearly polarized at higher frequencies. Four-component forms are rare in the radio pulsar population, whereas one finds hundreds of triple and scores of five-component profiles. For slower pulsars (rotation periods greater than 100 ms or so), the core-double cone beaming model provides a successful quantitative description for the vast majority of stars (ET VI, ET IX). Triple profiles then usually represent sightline traverses through one cone and the core, whereas five-component profiles reflect both cones and the core. The few available four-component profiles exhibit forms similar to those of five-component pulsars—but absent a central core feature owing either to weakness or to a sightline that just misses it (*e.g.*, B1738–08 in ET VI)—either case resulting in significant emission at the profile center. Also the inner conal component pair is generally weaker. Thus these four component sets do not appear

evenly spaced—but rather as clear leading and trailing pairs. The J0631+1036 21-cm profile is thus striking on all these grounds: the near even spacing of its four components; the deep emission minimum at the center; and the relative weakness of its outer component pair.

This is not all: also striking is the unusually complete fractional linear polarization of the 21-cm profile in Fig. 1 across almost the full width of the profile. Most radio pulsar profiles have substantial linear polarization, but nearly complete polarization is rare. Further, the accompanying polarization position-angle (hereafter PPA) traverse of J0631+1036 is no less remarkable, sweeping the greater part of the canonical  $180^\circ$  associated with a central sightline geometry, but in a strikingly asymmetric manner. Indeed, the steepest gradient point falls not near the profile center but on its far trailing edge, clearly suggesting that aberration/retardation (hereafter A/R) is a significant factor in its structure.

PSR J0631+1036 was discovered by Zepka *et al.* (1996), in the course of an Arecibo search targeted at *Einstein* IPC X-ray sources. It has a rotation period  $P_1$  of 0.288 sec and a spindown of  $1.05 \times 10^{-13}$  sec/sec, giving it a large magnetic field ( $5.6 \times 10^{12}$  G), acceleration potential (66.9) and rotational energy loss ( $1.7 \times 10^{35}$  ergs). The pulsar was also detected at  $\gamma$ -ray energies by the Fermi

\* Mateus.Teixeira@uvm.edu; Joanna.Rankin@uvm.edu

† G.Wright@sussex.ac.uk

‡ jinx@ncac.torun.pl

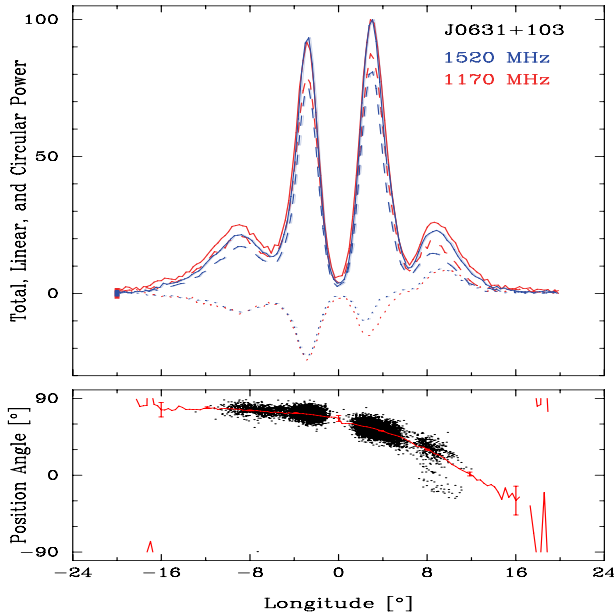


**Figure 1.** Overlaid average profiles at 1170 MHz (red) and 1520 MHz (blue), including polarimetry information (Stokes  $I$ , solid curve; linear  $[\sqrt{Q^2 + U^2}]$  dashed; and circular  $V$  dotted), for pulsar J0631+1036 on MJD 54540. The average PPA  $[\frac{1}{2} \tan^{-1} U/Q]$  traverse in the bottom panel corresponds to that of the three combined bands.

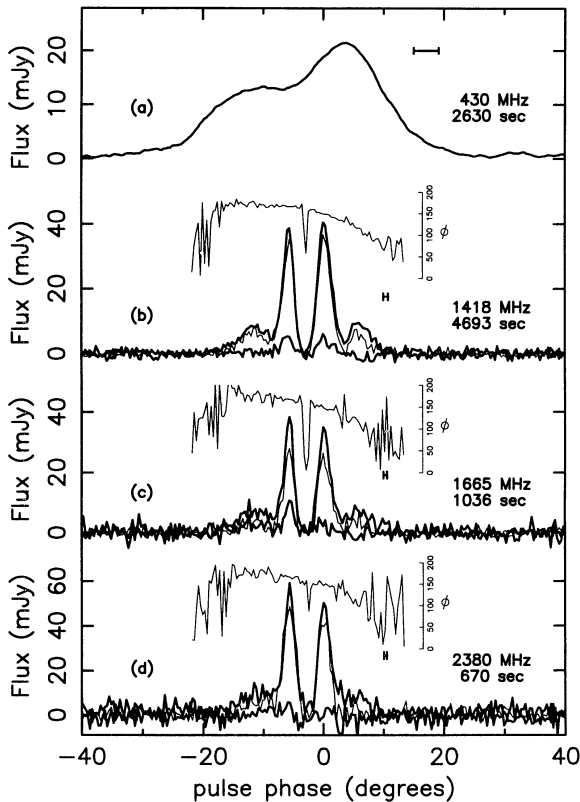


**Figure 2.** Zepka *et al.*'s (1996) fig. 3 showing the polarized profile forms at three frequencies and a 430-MHz total-power profile.

LAT Observatory (Weltevrede *et al.* 2010), and Seyffert *et al.* (2011) also discuss its interpretation. Such a high energy-loss rate (indeed, high energy detection!) and acceleration potential suggests that its emission might well be core dominated, but nothing about its profile form seems to support this interpretation. Figure 2 reproduces Zepka *et al.*'s fig. 3, where the pulsar's polarized profile can be seen at four bands between 430 and 2380 MHz.

Finally, the pulsar's evolution with frequency is also difficult to understand. At 430 MHz (Fig. 2, top), the J0631+1036 profile is much broader and has the form of an unresolved double. Such a profile evolution—that is, broader at longer wavelengths—is an expected aspect of outer conal emission; however, that the emission component number appears to change from one frequency to another—this is virtually unknown and deserves explanation.

It is known that this pulsar has unusually high dispersion (DM) and rotation (RM) measures for its position near the Galactic anticenter—suggesting a distance of 6.5 kpc, whereas its actual distance is probably around 1 kpc—and is therefore thought to be shrouded in a relatively dense environment, which is not its SNR of birth (Zepka *et al.* 1996). The star also experiences an exceptionally frequent number of glitches, often of non-standard nature (Espinoza *et al.* 2011). Might these unusual features be somehow linked to J0631+1036's strikingly unusual profile?

In preparing this report we have drawn on some new Arecibo observations as well as soliciting the widest possible range of theoretical opinions in an effort to understand and explain pulsar J0631+1036's multifrequency profiles. §II then presents the new observations and analyses §III then discusses the implications of this model theoretically. §§III–VI present different possible emission models and §VI provides an overall summary and discussion.

## II. DOUBLE CONE/CORE BEAM MODEL

### Morphology & Conal Spreading

The average profile of pulsar J0631+1036 develops remarkably over the three octaves of available observations, but the Zepka *et al.* profiles in Fig. 2 leave important questions unresolved: Their meter-wavelengths (430-MHz) total power profile seems to exhibit a resolved conal double (D) configuration (as per the classification in ET I & ET VI); however, it is also less well resolved than the others, and scattering may also be an issue. Further, the profiles appear to be time aligned, but the paper does not explicitly say so, and there is no low frequency polarimetry.

In order to resolve these issues we carried out Arecibo polarimetry observations at three bands in close succession on the same days. Two profiles from the MJD 56514 observation are shown in Figure 3. The 430-MHz profile (bottom panel) is better resolved than the Zepka *et al.* one and shows clear four-fold structure corresponding to the four components at 1.4 GHz (top panel). The 327-MHz profile (not shown), however, has only an un-

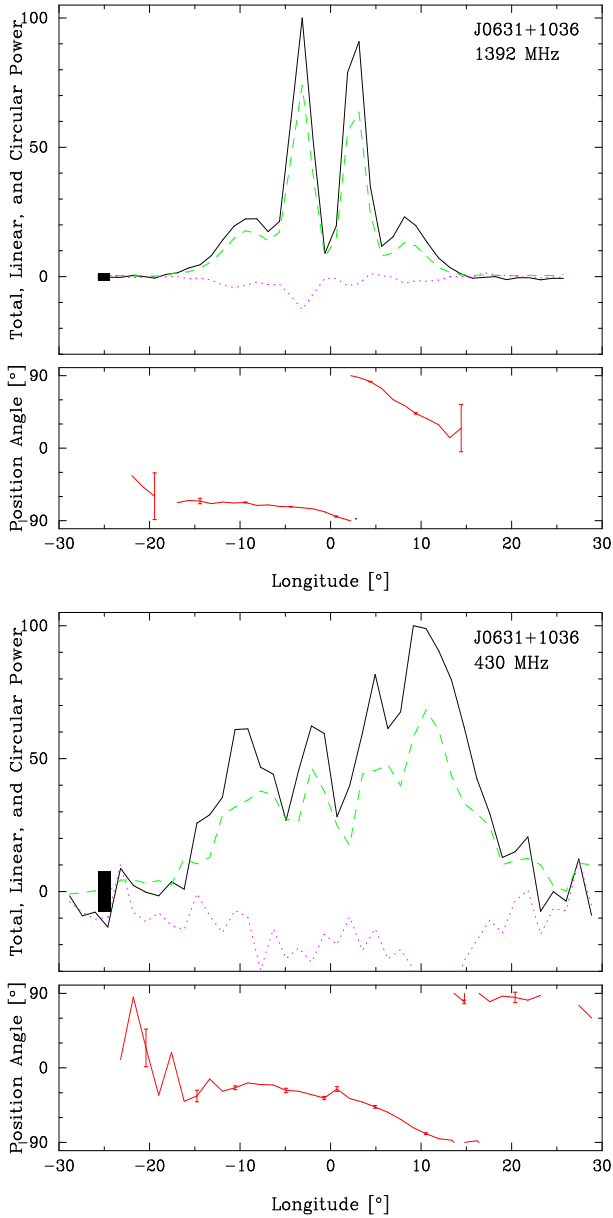


**Figure 3.** Profiles corresponding to two of the three frequency bands observed on MJD 56514: 1392 MHz (top) and 430 MHz (bottom) after Fig. 1. The four components of the star’s profile show clearly in this 430-MHz profile. Note also while the latter is much broader overall than at 1.4 GHz, the component peaks fall at very similar spacings—the inner cone spacing hardly altered and that of the outer conal components only 2-4° wider.

resolved double structure similar to that in the Zepka profile in Fig. 2. Figure 4 shows another 327-MHz profile from MJD 54016, where the four components also are conflated into an unresolved double form. Note, however, the increased breadth, depolarization and flattening of the PPA traverse on the trailing edge (at 430 MHz as well)—suggesting that the above authors were correct in attributing the low frequency broadening to scattering.

This said, we have found the star’s low frequency profiles somewhat variable from day to day. The four components in the 430-MHz profile of Fig. 3 are well

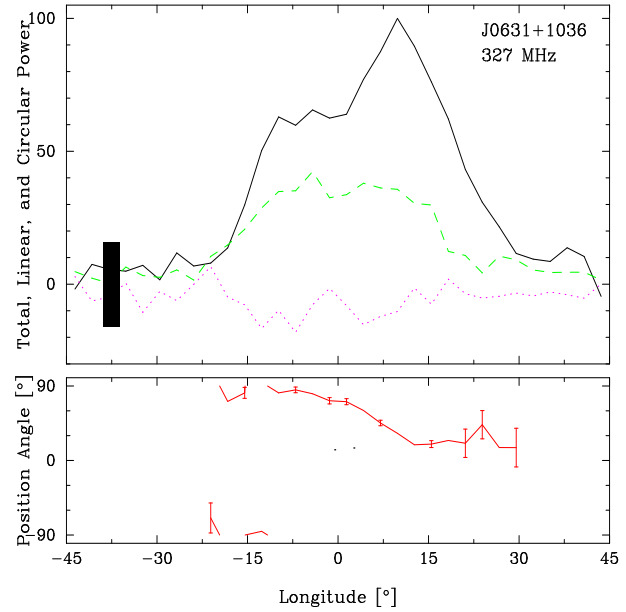


**Figure 4.** Polarized profile at 327-MHz from MJD 54016 after Fig. 1. Note the highly linearly polarized leading and depolarized trailing edges and the flattened trailing PPA traverse.

resolved; however a very similar observation two weeks earlier showed a profile much like that of Zepka *et al.*’s. Similarly, the unshown 327-MHz profile corresponding to those in Fig. 3 showed only moderate linear polarization which was uniform across the profile, whereas other 327-MHz observations show a highly polarized leading region and a depolarized trailing one as in Fig. 4.

These profiles then resolve any mysteries about J0631+1036’s profile evolution: the outer conal component pair strengthens relative to the inner one with wavelength, so that at meter wavelengths both pairs have comparable intensities—a trend that was discernible even in Figs. 1 & 2; and the four-fold structure at 327-MHz (and perhaps sometimes at 430 MHz) is conflated by scattering.

The full width at half maximum (FWHM) width for the 1520-MHz total power profile is some  $\sim 22.5^\circ$ , significantly narrower than the  $\sim 34^\circ$  FWHM of the 327-MHz profile, as would be expected for an outer conal emission geometry. By using our other profiles at 1170 and 1420 MHz and those of Zepka *et al.* at 430, 1665 and 2380 MHz (23.2, 22.0, 31, 21.5 and  $21^\circ$ , respectively) we were able to assemble the information for modeling in Table 1, where we see that the values exhibit the expected increase with wavelength.

FWHM values for the inner component pair, by contrast, change little with frequency as is expected for an inner cone, hovering around  $8.3^\circ$  and to perhaps  $9^\circ$  at 430 MHz. Moreover, the inner-conal component pair weakens with wavelength relative to the outer pair, again a typical behavior in double cone profiles.

Figure 5 then exhibits the star’s dramatic high frequency PPA traverse. In this 1520-MHz profile, we see a well resolved set of four highly polarized and symmetrical components, with near zero emission between the inner pair. The PPA swings through more than  $100^\circ$  with

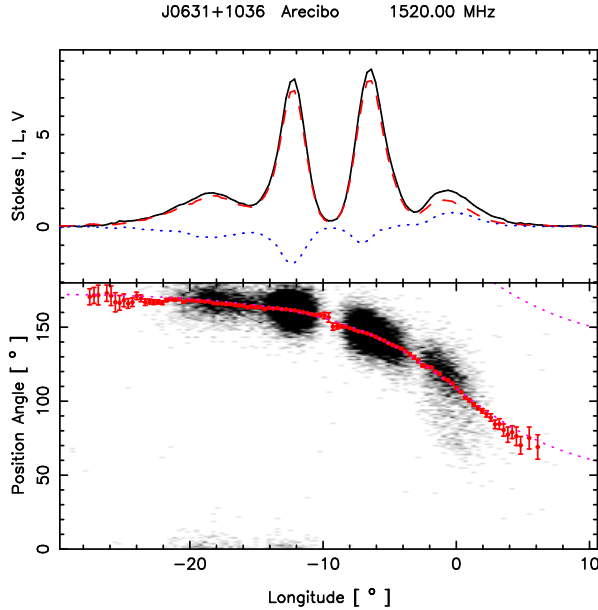


**Figure 5.** J0631+1036 1520-MHz profile and PPA fit (dotted magenta line, bottom panel). The longitude origin is taken at the fitted PPA inflection point and the fitted traverse corresponds to  $\alpha=36.5^\circ$  and  $\beta=-5.0^\circ$ , in the convention of ET VI. However, the latter values are highly correlated, so it is central slope  $R_{PA} [= \sin \alpha / \sin \beta]$  of  $-6.8 \pm 0.2^\circ / ^\circ$  that is significant.

**Table 1.** Double Cone Geometry Model for PSR J0631+1036.

| Freq<br>(MHz) | $w_i$<br>( $^\circ$ ) | $\rho_i$<br>( $^\circ$ ) | $w_o$<br>( $^\circ$ ) | $\rho_o$<br>( $^\circ$ ) | $\beta/\rho_o$ | $h_i$<br>(km) | $h_o$<br>(km) |
|---------------|-----------------------|--------------------------|-----------------------|--------------------------|----------------|---------------|---------------|
| 2380          | 8.3                   | 7.3                      | 21.0                  | 10.3                     | -0.65          | 103           | 204           |
| 1665          | 8.3                   | 7.3                      | 21.5                  | 10.4                     | -0.64          | 103           | 209           |
| 1520          | 8.3                   | 7.3                      | 22.0                  | 10.6                     | -0.63          | 103           | 215           |
| 1420          | 8.3                   | 7.3                      | 22.5                  | 10.7                     | -0.62          | 103           | 221           |
| 1170          | 8.3                   | 7.3                      | 23.2                  | 10.9                     | -0.61          | 103           | 230           |
| 430           | 9                     | 7.5                      | 31                    | 13.4                     | -0.50          | 107           | 343           |
| 327           | —                     | —                        | 34                    | 14.4                     | -0.46          | —             | 395           |

Note:  $\alpha$  is taken as  $52^\circ$  and  $\beta$  as  $-6.7^\circ$  (in the convention of ET VI), such that  $R_{PA} [= \sin \alpha / \sin \beta]$  is  $-6.8^\circ / ^\circ$ . The  $\beta/\rho_i$  column is omitted because its value never departs from  $-0.9$ .

the inflection point falling under the trailing component. Note that a very similar but less complete traverse is seen in Fig. 4—though its depolarized and flattened trailing region appears to reflect the effects of scattering.

A single-vector model (hereafter SVM) fit to the pulsar’s PPA traverse at 1520 MHz is also shown in Fig. 5 (dotted magenta curves). The four-parameter fit fixes the longitude origin at the steepest gradient (SG) point of the traverse. It also determines nominal values of magnetic colatitude  $\alpha$  and sightline impact angle  $\beta$ . However, these latter values are typically 99% correlated, so it is the PPA slope  $R_{PA} [= \sin \alpha / \sin \beta]$  at the SG point that is significant and well determined (see also ET IX). This value is  $-6.8 \pm 0.2^\circ / ^\circ$ .

**Table 2.** Aberration/retardation results for PSR J0631+1036.

| $\phi_l^i$<br>( $^\circ$ ) | $\phi_t^i$<br>( $^\circ$ ) | $\nu^i$<br>( $^\circ$ ) | $\rho^i$<br>( $^\circ$ ) | $r_{em}^i$<br>(km) | $s_L^i$ |
|----------------------------|----------------------------|-------------------------|--------------------------|--------------------|---------|
| Outer cone                 |                            |                         |                          |                    |         |
| -20.8                      | +1.3                       | -9.8                    | 10.6                     | 585                | 0.60    |
| (0.2)                      | (0.2)                      | (0.14)                  | (0.1)                    | (8)                | (0.01)  |
| Inner cone                 |                            |                         |                          |                    |         |
| -13.6                      | -5.4                       | -9.5                    | 7.4                      | 570                | 0.42    |
| (0.1)                      | (0.1)                      | (0.07)                  | (0.03)                   | (4)                | (0.01)  |

Note: The A/R height values do not depend on the emission geometry, but computation of the conal and “footprint” radii do. The  $\alpha$  and  $\beta$  values are taken as in Table 1.

### A/R Emission-Height Estimation

As we saw in the J0631+1036 profiles above, the star’s PPA traverse is so SVM-like and its SG point so dramatically delayed with respect to the profile center that the situation seems almost to scream out for A/R analysis. Not so fast, however! The physical basis and practical application of A/R analysis was first developed by Blaskiewicz *et al.* (1991; hereafter BCW), but only over the last decade or so has it found wide application and provided increasingly consistent results. Fundamental to all A/R analyses is reliable determination of a profile center which can be interpreted as the longitude of the magnetic axis. Such interpretations have followed one of two courses: a) taking the midpoint between two conal components as relative to the PPA SG point as falling symmetrically on either side of the magnetic axis longitude (BCW), or b) taking the center of a core component as marking the magnetic axis longitude [Malov & Suleymanova (1998) and later Gangadhara & Gupta (2001), hereafter G&G].

Pulsar J0631+1036’s unusual profile above, however, gives us pause. While we do see evidence that the star’s four components represent inner and outer conal component pairs, we do not want to rush to this conclusion. However, their striking symmetry remains—as well as the striking asymmetry of the PPA traverse—and it is very hard to understand how the longitude of the magnetic axis could fall at any other point than midway between the centers of the two conal component pairs and the PPA SG point.

So emboldened, we have conducted an A/R analysis of the former type. However, in terms of computations, all are the same, and the values in Table 2 are similar to tables in previous such efforts in G&G, Srostlik & Rankin (2005), Force & Rankin (2010) or Mitra & Rankin (2010) and are corrected as advised by Dyks, Rudak, & Harding (2004).  $\phi_l^i$  and  $\phi_t^i$  are the respective leading and trailing longitudes of the centers of one or the other component pairs;  $\nu^i$  is the computed center of the pair;  $\rho^i$  is the computed radius of the emission cone; and  $r_{em}^i$  and  $s_L^i$  give the physical emission height and relative polar cap annulus, respectively.

The Table 2 results are interesting but strange. The computed physical emission heights of some 600 km for

the putative inner and outer cones are indistinguishable within their errors. Physical heights in the 450-600 km range at 1 GHz are expected for outer cones, but those of inner cones are usually substantially less. Moreover, the emission annuli traced down to the polar cap seem both too close to one another and too well determined.

Finally, we note that the symmetry of the component properties (broad, thin, thin, broad), as well as their separation, is unexpected in terms of Dyks *et al.* (2010a). Even with all components at the same height, A/R would tend to lend some degree of asymmetry to components intrinsically symmetric about the profile centre [producing either bb tt or tt bb]; however, this effect has not been identified as yet in any pulsar .

### Quantitative Geometry

The most accurate and consistent estimates of a radio pulsar’s emission geometry—that is, its magnetic colatitude  $\alpha$  and sightline impact angle  $\beta$ —result from using *both* the angular width information of its profile and the sightline-path information in its PPA traverse. This was the method used in ET VI (Rankin 1993) wherein the bulk of the population with then well measured polarization profiles were found to exhibit a core and double-cone structure—that is, with a half-power core width of  $2.45^\circ P^{-1/2}$  and outside half-power conal radii of  $4.3^\circ P^{-1/2}$  and  $5.8^\circ P^{-1/2}$  (all at 1 GHz), respectively.<sup>1</sup> And these conal radii then imply *characteristic* emission heights of some 130 and 220 km, respectively.<sup>2</sup>

Pulsar J0631+1036’s profile had seemed so unusual that we were slow to assess whether it might represent an inner and outer conal component pair. However, as we have seen in the foregoing sections, the actual properties of this profile—its frequency evolution and PPA traverse—in fact largely appear compatible with this interpretation. What remains then is to ask whether such a geometry is consistent quantitatively. No core feature is discernible at any frequency for this pulsar, so we have no independent means of estimating the pulsar’s magnetic colatitude. However, we can ask whether there is any value of  $\alpha$  such that the two putative emission cones have their expected dimensions.

Table 1 gives such a double-cone geometric model for J0631+1036. The model values of  $\alpha$  and  $\beta$  are taken as  $52^\circ$  and  $-6.7^\circ$ , such that the PPA sweep rate  $R_{PA}$  is

<sup>1</sup> Lyne & Manchester (1988) carried out a similar geometric study and came to many similar conclusions. They also identified a group of some 50 so-called ‘partial cone’ pulsars that appeared not to exhibit core/conal structure. Reinvestigation of this population using new observations, however, has shown that the vast majority exhibit a core/double-cone profile structure with the above dimensions (ET IX).

<sup>2</sup> Such *characteristic* emission heights are not to be confused with actual, physical emission heights. In the ET VI context, computation of emission heights entails association of the conal emission outer boundary (for both inner and outer cones!) with the “last open” field line. Clearly this is an implausible circumstance physically; its use, however, provides a consistent outer boundary for emission along the edges of the polar flux tube.

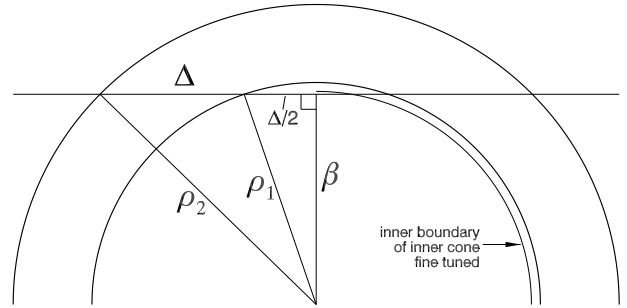


**Figure 6.** Viewing geometry for a profile with four equidistant components. The horizontal line is the path of a sightline cutting through a beam consisting of two coaxial cones with the size ratio of  $\kappa = \rho_1/\rho_2$ . The impact angle  $\beta$  and the separation of components  $\Delta$  are marked. Note the fine tuning required to obtain the equidistance, and the extremely small thickness of the inner side of the inner cone, required to observe the low-flux central minimum.

$-6.8^\circ$  as determined from Fig. 5. The respective inner and outer conal radii are computed according to ET VI eq. (4) and the emission heights per eq. (6). Only for this last computation is the pulsar’s rotation period  $P_1$  (0.288 s) used to estimate the angular size of the star’s polar cap so that magnetic-polar colatitudes can be related to *characteristic* emission heights.

More or less reasonable conal dimensions and characteristic heights are obtained using the model in Table 1 for  $\alpha$  values between about  $50^\circ$  and  $60^\circ$ . For  $\alpha$  near the upper value, the inner cone exhibits its expected radius and height, and for the lower value the outer cone assumes a radius such that the model 1-GHz *characteristic* emission height is about the expected 220 km. The table is computed for an  $\alpha$  of  $52^\circ$ . The lack of simultaneously appropriate conal dimensions for a single  $\alpha$  value is unusual, but otherwise the model is not unsatisfactory.

As a whole then, the profile morphology of J0631+1036 suggests that it is a member of the conal quadruple (cQ) class (ET VI). Moreover, if the above geometry is correct, there are at least two reasons why no core component is seen in the profile: a) the radius of the core component would be some  $2.28^\circ$ , whereas  $\beta$  is  $-6.7^\circ$ , so the Gaussian-shaped core-beam power would be attenuated by a factor of about 5000; b) what power remains would appear not in the empty profile region between the two inner conal components, but rather halfway between this point and the PPA SG point, at some  $-4.9^\circ$  longitude in Fig. 5, where it would be conflated with power from the trailing inner conal component. This said, the model shows that  $\beta/\rho_i$  is  $-0.9$  for the inner cone, and it is very hard to understand how the two inner conal components could be so narrow and well resolved in this configuration – a matter that is explored further below.

### Geometry of nested cones with equidistant components

**In this section we further demonstrate**, on purely geometric grounds, that the nested-cone structure inferred for this pulsar is highly unnatural: the near-zero flux at the centre and the nearly equal distances between

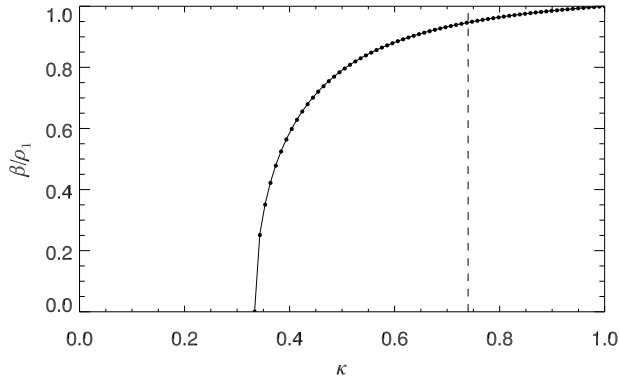


**Figure 7.** The value of  $\beta/\rho_1$  as a function of the cone size ratio  $\kappa$  for profiles with equidistant components. The curved line represents the flat solution (eq. 2). The dots present the numerical solution for spherical case. The dashed vertical marks the frequently observed value of  $\kappa$  (Wright 2003). This case is illustrated in the previous figure.

components ( $\Delta \approx 6^\circ$ ) require fine-tuned geometry with a strange ratio of cone radii and an extremely thin inner cone.

This can be proved by considering the flat geometry shown in Fig. 6. The two semicircles represent the maxima of emission cones. Our line of sight crosses them along the horizontal line. The ratio of the angular radii of the two cones is  $\kappa = \rho_1/\rho_2$  (shown here as 0.74), and  $\Delta$  is the separation between the peaks in the profile. Two Pythagorean theorems can be written for the two right-angled triangles:  $(\rho_1, \Delta/2, \beta)$  and  $(\rho_2, 3\Delta/2, \beta)$ , and solved for  $\Delta$  and  $\beta$ :

$$\frac{|\Delta|}{\rho_1} = \left( \frac{1 - \kappa^2}{2\kappa^2} \right)^{1/2}, \quad (1)$$

$$\frac{|\beta|}{\rho_1} = \left( \frac{9\kappa^2 - 1}{8\kappa^2} \right)^{1/2}. \quad (2)$$

The two quantities depend only on the ratio  $\kappa$  of the cones' size. In the exact spherical case, when the line of sight is tracing a circle around the rotational pole, eq. (1) becomes modified: for a single value of  $\Delta$  there exist two solutions for  $\rho_1$ , and two solutions for  $\beta$  (one positive and one negative, and of slightly different absolute value). However, numerical solution of the problem in spherical geometry suggests that for both values of  $\beta$ , eq. (2) remains intact (Fig. 7). Thus, in the spherical case  $\beta$  and  $\rho_1$  scale in such a way that the simple equation (2) is preserved, with no additional dependence on  $\alpha$  or  $\Delta$  involved.<sup>3</sup> In what follows, eq. (2) will then be considered valid in general.

As can be seen in Fig. 6, in the nested cone model doubly fine-tuned conditions need to hold to generate the profile with equidistant components and deep central minimum. First, for a reasonable cone size ratio ( $\kappa \gtrsim 0.5$ ) the impact angle  $\beta$  must be a precise fraction of  $\rho_1$ . Since  $\beta/\rho_1$  changes very slowly with  $\kappa$  (for  $\kappa \gtrsim 0.5$ ), even a small mistuning in  $\beta$  does not result in the equidistance.

<sup>3</sup> How to prove this analytically?

Second, to produce the equidistance, the line of sight must almost be grazing the very edge of the inner cone (Fig. 6). Wright (2003) has argued that both observational (Rankin 1993) and theoretical arguments support the value  $\kappa = 0.74$ , for which  $\beta/\rho_1 = 0.95$ . Thus, for the cone ratio typically found in statistical studies, the line of sight passes very close to the edge of the innercone.<sup>4</sup> This implies that to observe the central minimum with the flux almost disappearing, the inner boundary of the inner cone (where the intensity almost vanishes) needs to be very close to the cone's peak, as marked in Fig. 6 with the thin quarter-circle arc. The location of this inner boundary needs to be extremely fine-tuned to reproduce the low flux at the centre of the profile.

Moreover, each inner-pair component has a roughly symmetric triangular shape, which would require a special, asymmetric emissivity profile of the inner cone, with the intensity dropping much faster on the inner side than on the outer side of the inner cone. Indeed, by matching the 1.5-GHz profile with Fig. 6, the inner half-thickness of the inner cone can be estimated to  $(\delta\rho_1)_- \simeq \rho_1 - \beta = 0.05\rho_1$ , whereas the the outer half-thickness of the inner cone is roughly equal to  $(\delta\rho_1)_+ \simeq (\rho_2 - \rho_1)/2 = 0.17\rho_1$ , which is considerably larger than  $(\delta\rho_1)_-$ .

The traditional nested-cone geometry can then be considered unacceptably fine tuned. The geometry invoked within the nested-cone model seems to be more contrived than we would expect based solely on the low statistics of such quadruple-and-symmetric profiles.

The situation does not improve for a smaller cone ratio of  $\kappa = 0.5$ , because  $\beta/\rho_1 = 0.79$  is still quite large in this case. The equidistance condition implies that the smallest possible cone ratio is  $\kappa = 1/3$ , for which  $\beta = 0$ , *i.e.* the line of sight is cutting through the cone centrally. However, this case is probably excluded by the limited slope of the polarisation angle curve. Therefore, the reasonable range of cone ratio for J0631+1036 can be limited to a quite narrow range:  $\kappa \in (0.35, 0.5)$ . We can basically say that for the nested cone model, the ratio between the angular radii of cones in J0631 is around 0.4. This is much smaller than the typical value of 0.75. The value of  $\beta/\rho_1$  is not tightly constrained, because the relation  $\beta(\kappa)$  is steep around  $\kappa = 0.4$  (see Fig. 7). The most likely value of  $\beta$  is somewhere between 0 and  $0.7\rho_1$ .

It is concluded that for the equidistant profile, the deep central minimum must result from either a very special cut through extremely thin inner cone with strange emissivity profile, or from a peculiar conal structure that has uncommon cone size ratio. It would seem that an alternative to the classic double-cone model must be found for this pulsar.

<sup>4</sup> By 'passing near the edge of the inner cone' we mean the passage which is nearly tangent to the mathematical cone corresponding to the *peak* flux of the inner components, not to be confused with the low-intensity boundary of the cone, discussed below.

#### IV. ALTERNATIVE EMISSION MODELS

Such difficulties tempt us to consider other geometries. First, in the next section (§V), we ask if any model can be found which sees some of the profile components of J0631+1036 as being generated by radiation from down-flowing particles on the far side of the pulsar. Down-flow has occasionally been discussed in other pulsars but as yet not convincingly (e.g. in B1822–09, Dyks *et al.* 2005b). Nevertheless, in the context here such a model would still be based on a conal radius-to-frequency mapping (RFM), a feature which seems to serve us reasonably well in many regular pulsars, and the symmetry of the model might naturally account for the most dramatic feature of J0631+1036: its near-symmetric profile.

A second approach is to insist that the observed radio emission arises entirely on the nearside of the pulsar, so that the observed profile and PA swing is produced by non axially-symmetrical beam geometries. For example, in an alternative to the hollow cone picture, one can ask if both the central minimum and the four-peak symmetry can be inherent features of the beam, independent of the viewing angle. In §VI we consider a cut through a four-lobed plane-symmetric beam, with the deep central minimum extending over a wide range of magnetic colatitudes.

#### V. BIDIRECTIONAL (UP/DOWNFLOW) EMISSION MODELS

##### Models with emission at a common height for each frequency

The notion of detecting downflow on the reverse side of a pulsar as radio emission in a variety of different configurations was provoked by phenomena such as double features and notches (Dyks *et al.* 2010b) or unusual precursor features (Dyks *et al.* 2005a,b). In J0631+1036 an obvious step would be to assign two of its peaks to nearside emission and two to farside. One way to do this would be to assume that components 1 and 3 are emitted from a nearside cone, 2 and 4 from a farside cone, so that all components at a given frequency are emitted at the same altitude on exactly the same dipolar fieldlines on both the near- and farside of the pulsar and are symmetric about the magnetic axis

Given the known component separations, It is an elementary matter to estimate the implied common height ( $\approx 360km$ ) at which the components are emitted. This height is quite plausible, but neither the near- or farside emission places the SG at its observed position (under component 4). If we try locating components 1 and 2 on the nearside and 3 and 4 on the farside we again obtain a not implausible emission height ( $\approx 720km$ ), but the expected location of the SG is still not compatible with the observed position.

For these and other reasons (it is difficult to account for the fat and thick sequence (fttf) of the components) these models have to be rejected: it is already clear that the observations are placing severe constraints on possible models.

#### Twin beam model

A further scenario within the context of bidirectional flow presents itself if we focus on the emission from the broader but weaker outer components of J0631+1036 and temporarily ignore the inner components. Let us suppose that these arise from identical single beams at either pole (Fig 8), each forming a narrow axisymmetric cone about the pulsar’s magnetic axis. Then the outer components of J0631+1036 are the frequency-dependent manifestation of the upward nearside and downward farside emission at a particular height, and our sightline comes closest to the magnetic axes at this height at the component centres.

In this configuration the profile centre is again identified as the fiducial point, and a simple computation of the emission height now gives  $\approx 600km$  – again a reasonable value. However, the standard Blaskiewicz *et al.* (1991) rule now implies that the nearside emission (component 1) has its maximum PPA swing (SG) at the phase component of component 4, exactly where it is observed in the profile. This makes the model interesting, although it would imply that the SG of the *downward* flow should appear reflected at the phase of component 1, which is definitely not seen. This model therefore requires us to argue (as implied by Johnston & Weisberg 2006) that the farside emission acquires the properties of the nearside emission as it propagates through the open fieldlines of the nearside magnetosphere.

We then need to account for the profile’s central components. If they arise from within the beam, A/R implies that their emission sites must lie close to the pulsar, on the far and nearside, and at heights of about 360 km (Fig. 8). We suggest that they may arise as caustic effects, so that intrinsically weak emission is boosted to detectable levels by the geometric coincidence of our line of sight moving instantaneously parallel to the trajectory of the emitting particles (see Dyks *et al.* 2010 for a study of this effect in rapidly rotating pulsars). It is possible to produce a set of parameters corresponding to a narrow beam (i.e. a low polar footprint parameter  $s$ ) and plausible angles of inclination which might generate a caustic effect. Furthermore, the caustic effect can be expected to diminish at lower frequencies as the appropriate fieldlines no longer lie within the beam and the separation between components 1 and 4 expands.

One may reasonably object that neither strong caustic effects nor downflow emission have yet been identified in other relatively slow pulsars, so this model is highly speculative in nature. Nevertheless, it does retain the basic pulsar features of a conical beam with radius-to-frequency mapping.

#### VI. WEDGE-SHAPED MODELS

The models assume that the emission region, when viewed down the dipole axis, resembles a wedge-shaped piece of a round birthcake (Fig. 9). The corresponding beam covers a limited range of magnetic azimuths and is intrinsically structured in the form of the four azimuths of enhanced emission (solid contours in Fig. 9). It is as-

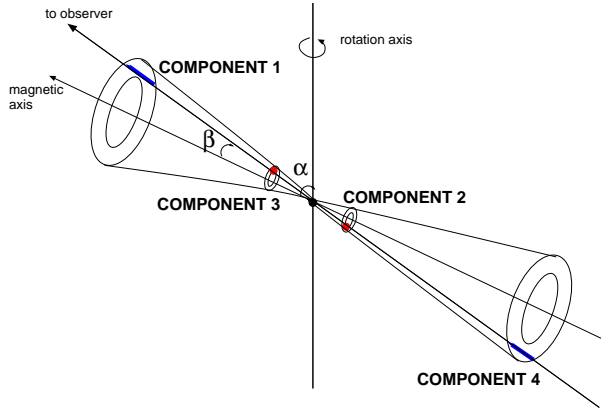


**Figure 8.** The twin beam model for J0631+1036. The observer sees the principal upward emission from a conical beam on the nearside in component 1 and downward emission from component 4, both at a height of about 600 km. As the pulsar turns, caustic effects are seen in the leading half of the profile at component 2 generated by low altitude downward emission on the farside of the pulsar, followed by component 3 in the trailing half from equivalent emission on the nearside close to the star.

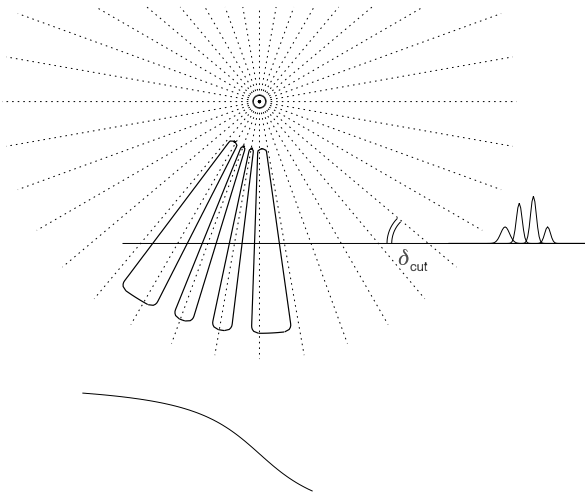


**Figure 9.** Top view of the radio emission region (beam) at 1.5 GHz (solid contours). The beam consists of four lobes which are symmetric with respect to a plane that does not coincide with the main meridian. The radially spreading dotted lines mark the B-field lines viewed down the dipole axis. The horizontal solid line marks the passage of the line of sight. The expected pulse profile is shown on the right hand side, and the asymmetric PA curve below the beam.

sumed that the symmetric fourfold structure is inherent to the physics or geometry of the emission process or region itself. As shown<sup>5</sup> in Fig. 9, the region is not centered

<sup>5</sup> Actually the  $\vec{\Omega}$ -axis is not shown in the figure. The vertical orientation of the meridian is implied by the horizontal trajectory of the line of sight.

at the main meridian fixed by the rotation axis  $\vec{\Omega}$  and the dipole axis  $\vec{\mu}$ . The region’s altitude is assumed to not exceed a few stellar radii, so that effects of corotation do not contribute significantly to the observed delay of PA curve. For the rotation period of J0631+1036 ( $P = 0.288$  s), the rotationally-induced PA shift reaches 10% of the observed value ( $\sim 1^\circ$ ) at the altitude of  $6 \cdot 10^6$  cm, which is an estimate for a maximum height below which the rotational effects in J0631+1036 can be neglected.

The wedge geometry of Fig. 9 has a few properties consistent with the observations:

1. The large delay of the PA curve finds automatic explanation in the off-meridional location of the emission region. There may be some small contribution of the corotational PA shift, but we assume that the spatial offset does dominate.

2. The leadingmost component (no. 1) is cut by the line of sight at a smaller angle than the trailingmost component (no. 4), which is cut almost orthogonally. Therefore, the 1st component is noticeably wider than the 4th one: the observed 1.5-GHz widths are:  $W_1 \simeq 8^\circ$ , and  $W_4 \simeq 6^\circ$ . Note that the asymmetry of the component’s width is assumed to be fully determined by the local viewing geometry (the angle at which the line of sight is cutting through each component), not by the AR effects which, for simplicity, are assumed negligible in the wedge model.

3. The structured-wedge shape ensures  $\nu$ -independent separations of components (no “RFM”), because the components are observed when the line of sight is crossing the appropriate magnetic azimuth, regardless of frequency. This is consistent with the weakness of RFM between 0.3 and 1.4 GHz (Figs. 3 and 4). In the 327-MHz profile the peak-to-peak width of the outer conal pair is close to  $19^\circ$ , ie. it is nearly identical to the 1.5 GHz value. The peak-to-peak RFM can thus be considered marginal, given the differences in morphology and the lower resolution of the low-frequency data.<sup>6</sup>

4. For the wedge-shaped geometry, the near-zero flux at the center does not require the fine-tuned viewing geometry shown in Fig. 6 (we suspect that the near-zero flux at the center would be observed also for different viewing angles).

To establish whether the model can reproduce the width, PA slope, and the small asymmetry of the outer components, we need a formula for calculating the observed pulse longitude for emission from a fixed magnetic azimuth.

### Profile width for wedge-shaped emitters

Let  $\theta_m$  (the magnetic colatitude) be the angle between the emission direction and the dipole axis, and  $\phi_m$  – the azimuth of the emission direction. The value of  $\phi_m$  is

<sup>6</sup> The magnitude of the RFM defined by the 50% outer envelope is different from the RFM based on the peak-to-peak separation that is discussed with regard to the wedge model. In particular, the magnitude of the FWHM-based RFM is enlarged by scattering tails that dominate the trailing side of the profile of J0631+1036 below 430 MHz.

measured around the dipole axis, with  $\phi_m = 0$  at the equatorward part of the main meridian. In the nested-cone model the magnetic colatitude  $\theta_m$  is fixed, whereas the magnetic azimuth  $\phi_m$  that is sampled by the line of sight at  $\theta_m$  as well as the observed pulse phase  $\phi$  are determined by the global geometric parameters: the dipole inclination with respect to the rotation axis  $\alpha$  and the viewing angle  $\zeta$ .

In the case of emission from fixed magnetic azimuth  $\phi_m$ , it is the magnetic colatitude  $\theta_m$  and the observed phase  $\phi$  which are determined by  $\alpha$  and  $\zeta$ . For a wedge-shaped emission region that is symmetric with respect to the main meridian, the width of profile is  $W = 2|\phi_l| = 2\phi_t$ , where  $\phi_l$  and  $\phi_t$  is the observed phase of the leading and trailing edge of the profile, assumed to be measured from the center of the profile. In the case of J0631, the trailing side of the profile is close to the fiducial plane so we have  $\phi_t \sim 0$  and  $W = \phi_t - \phi_l \simeq |\phi_l|$ . The value of  $\phi_l$  can be calculated with the use of spherical trigonometry, and there is a few ways to do this. Hereafter, we will neglect the index  $l$  at  $\phi$ , because the solution is symmetric with respect to the fiducial meridian.

A convenient way is to use the cosine theorem:  $\cos \zeta = \cos(\pi - \phi_m) \sin \alpha \sin \theta_m + \cos \alpha \cos \theta_m$  (Dyks Rudak & Demorest 2010b), which leads to the following quadratic equation for  $\cos \theta_m$ :  $A \cos^2 \theta_m + B \cos \theta_m + C = 0$ , where:

$$A = \cos^2 \alpha + \cos^2 \phi_m \sin^2 \alpha \quad (3)$$

$$B = -2 \cos \alpha \cos \zeta \quad (4)$$

$$C = \cos^2 \zeta - \cos^2 \phi_m \sin^2 \alpha \quad (5)$$

If the combination of  $\phi_m$ ,  $\alpha$  and  $\zeta$  is appropriate, the discriminant  $\Delta$  is positive, and there are two solutions for  $\theta_m$  which are measured from the same magnetic pole. The corresponding two values of the observed pulse phase can be calculated from another cosine theorem:

$$\cos \phi = \frac{\cos \theta_m - \cos \alpha \cos \zeta}{\sin \alpha \sin \zeta}, \quad (6)$$

which is normally used also for conal beams.

### Probing the parameter space for J0631+1036

In the case of J0631+1036, the value of maximum polarisation angle gradient  $R_{PA}$  is between  $-7$  and  $-5$ , depending on the frequency. Therefore, the method of the previous section will be applied for  $\alpha$  and  $\zeta$  related to always fulfill  $R_{PA} = \sin \alpha / \sin \beta = -6$ , where  $\beta = \zeta - \alpha$  is the impact angle.

To fully probe the parameter space we calculate the pulse width  $W \simeq \phi$  as a function of dipole tilt  $\alpha$  for a set of values  $\phi_m = 10^\circ, 20^\circ, 30^\circ$ , etc. The result is shown in Fig. 10. For small  $\phi_m \ll 1$  rad (and a fixed PA slope  $|\sin \alpha / \sin \beta| \gg 1$ ) the width of a profile does not much depend on  $\alpha$  (bottom curves). A simple estimate shows that the nearly  $\alpha$ -independent width of profile is equal to

$$W = |\phi(\phi_m)| \approx \left| \frac{\sin \beta \tan \phi_m}{\sin \zeta} \right| \simeq \frac{|\phi_m|}{|R_{PA} + \cos \alpha|} \sim \frac{|\phi_m|}{|R_{PA}|}, \quad (7)$$

where on the right-hand side we have made the approximation  $\cos \alpha = 0$ , which is reasonable when the polarisation curve is steep ( $|R_{PA}| \gg |\cos \alpha|$ ).

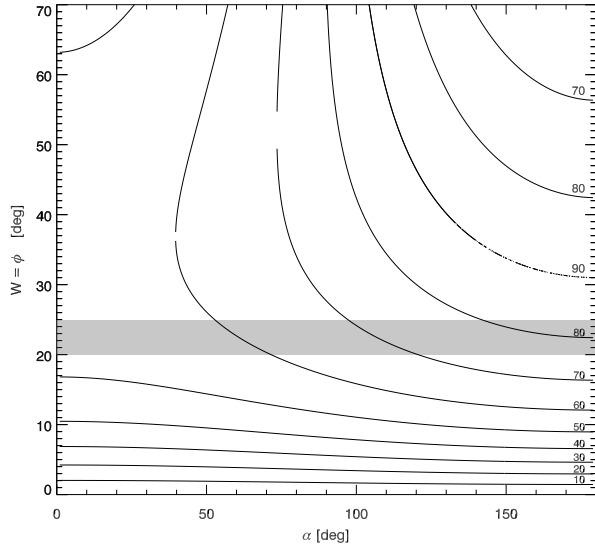


**Figure 10.** Pulse width  $W = \phi$  for a wedge-shaped emission region that occupies only the leading side of the fiducial meridian. The region extends between  $\phi_m = 0$  and  $|\phi_m| = 10^\circ, 20^\circ$ , etc. (bottom to top, see the numbers on the right hand side). The result has been obtained for central PA slope of  $\sin \alpha / \sin \beta = -6$ . The grey band presents the observed profile width.

Unlike in the conal scenario, where  $W$  can be arbitrarily enlarged by assuming smaller  $\alpha$  and  $\zeta$ , for small  $|\phi_m|$  and large  $|R_{PA}|$  the width of profile does not depend on the viewing parameters  $\alpha$  and  $\zeta$ . In the wedge model with a fixed PA slope, it is not possible to get a wider profile for smaller dipole inclination  $\alpha$ , because to keep the PA slope close to  $|R_{PA}| = 6$ , the impact angle  $\beta$  needs to be decreased accordingly, and the width of the emitting wedge near the dipole axis is narrower. This cancels out the small- $\alpha$  broadening and precludes the increase of the profile width  $W$ . Thus, a crucial difference between the conal emitter, and the wedge-shaped one, is that in the conal case the profile can be made wider through a decrease of the impact angle  $|\beta|$ , whereas in the wedge case the profile does not change or can even become narrower (Fig. 10,  $\alpha \rightarrow 180^\circ$ ).

Since the observed profile width of J0631 at high-frequencies is  $20^\circ - 25^\circ$ , the magnetic azimuth for the leadingmost component is between  $53^\circ$  and  $83^\circ$  (Fig. 10). This spread of magnetic azimuths is roughly consistent with the range of polarisation angles spanned by the PA curve (about 1 rad at 0.4 GHz, and  $\sim 100^\circ$  at 1.4 GHz).

The asymmetry of widths of components 1 and 4 is  $W_4/W_1 \sim 6^\circ/8^\circ = \sin \delta_{\text{cut}}(1)/\sin \delta_{\text{cut}}(4)$ , where  $\delta_{\text{cut}}(1)$  is the ‘cut angle’ between the sky-projected path of our sightline and the fixed-azimuth plane that corresponds to the component no. 1. Definition of  $\delta_{\text{cut}}$  is shown in Fig. 9. For the ‘near-meridional’ component 4 we have  $\sin \delta_{\text{cut}}(4) \sim \sin 90^\circ \sim 1$ , which implies that  $W_4/W_1 \simeq \sin \delta_{\text{cut}}(1) \simeq 0.75$ . Thus, the cut angle for component (1) is about  $\delta_{\text{cut}} \simeq 48^\circ$ . Note that much smaller cut angles are definitely excluded, because they would produce much stronger asymmetry of components. The function  $\delta_{\text{cut}}(\alpha)$  is shown in Fig. 11. It has been calculated for

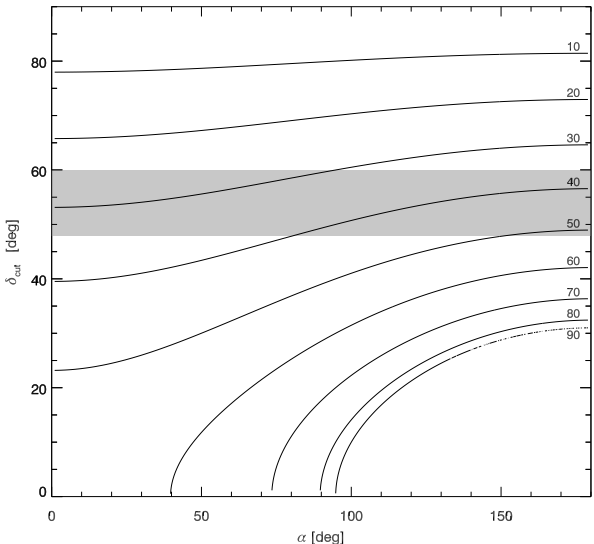


**Figure 11.** The cut angle  $\delta_{\text{cut}}$  as a function of dipole tilt  $\alpha$  for the fixed PA slope  $R_{PA} = -6$ . The grey band presents the observed value of  $\delta_{\text{cut}}$ . Note the lack of solutions for  $\phi_m \sim 90^\circ$  and small  $\alpha$ .

the previously mentioned set of  $\phi_m$  using eq. (6) in Dyks & Rudak (2012). The cut angle invoked from the observed asymmetry of components ( $\delta_{\text{cut}} \sim 48^\circ - 60^\circ$ ) implies  $\phi_m = 25^\circ - 51^\circ$ , which does not overlap with the range  $53^\circ - 83^\circ$ , derived above from the pulse width.

Thus, the wedge model is incapable to simultaneously reproduce the width of the pulse profile and the observed asymmetry of components 1 and 4. For the observed PA slope, the observed pulse width favours large  $\phi_m$  (wide wedge) whereas the small asymmetry of components suggests small  $\phi_m$ .

Fig. 10 makes it clear that for moderately narrow wedge ( $\phi_m < 50^\circ$ ) the resulting profile width is very small (typically less than  $\sim 20^\circ$ ). Wide profiles appear for larger values of  $\phi_m \gtrsim 60^\circ$ . However, this is simply the case when the whole quadrant of the polar cap starts to be filled-in, and the wedge transforms into the ‘half-filled polar beam’ case, in which either the leading, or the trailing side of polar tube is active. We conclude that models based on the narrow wedge geometry are incapable of producing even moderately wide profiles (with  $W \sim$  a few tens of degrees) in the presence of a steep slope of the PA curve ( $|R_{PA}| \gtrsim$  a few).

To save the wedge model, one is tempted to give up the idea that the PA has anything to do with the direction of dipolar B-field. Unfortunately, the association of PA with the projected B-field is inherent to the interpretation of the PA-curve shift that the model was devised to explain. This is not the first time when interpretation of polarisation angle data in terms of the rotating-vector model is suspected to be misleading (see Guillemot et al. 2013).

Another way to rescue the model, is to assume that the four lobes of the emission beam do not follow the geometry of the fixed magnetic azimuth. Instead, the lobes can keep the same distance from the central azimuth of the beam, without the radial merging close to the dipole

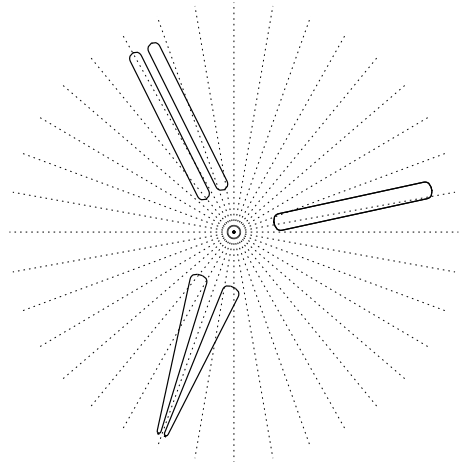


**Figure 12.** Sky-projected patterns of azimuthally-limited pulsar beams. The bottom pattern corresponds to the curvature radiation emitted by a plasma stream outflowing at a single magnetic azimuth. The beam emitted at lower altitudes (closer to the dipole axis) is wider than the beam emitted at larger  $r$ . This is because the opening angle  $\theta_{\text{cr}}$  of the double-lobed curvature beam decreases with increasing radius of curvature  $\rho$  of B-field lines ( $\theta_{\text{cr}} \propto \rho^{-1/3}$ ).

axis (top half of Fig. 12). A new observational support for the idea that pulsars really possess this type of stream-like emitters, has recently been provided by Desvignes et al. (2012), who analysed the relativistically precessing pulsar J1906+0746. Its main pulse emission seems to originate from an elongated stream deflecting away from the dipole axis, with its radio beam having roughly the same lateral width at different  $\theta_m$ , ie. not widening with the distance from the dipole axis. In such a case, the profile width can be calculated using eq. (4) in Dyks & Rudak (2012), with  $\Delta$  understood as  $W$ . We will not perform such modelling for J0631, because of the increased number of unknown parameters: multiple solutions are possible because the intrinsic angular width of the beam and the central azimuth  $\phi_m$  are unknown.

Geometry of similar type, albeit with the wedge-type beam *widening* close to the dipole axis, actually occurs for some physical processes that produce two-lobed emission beams. For example, it is the case for the split-fan beam of the curvature radiation (CR), shown in the bottom half of Fig. 12. The width of the CR beam increases for decreasing radius of curvature of electron trajectories  $\rho$ , according to:  $\theta_{\text{cr}} \propto \rho^{-1/3}$  (Jackson 1975). For emission from an outflowing thin plasma stream, the beam is wider closer to the dipole axis, where  $\rho$  is smaller, and becomes narrower with increasing radial distance  $r$  and  $\theta_m$  (Fig. 12). However, the CR beam is very narrow ( $2\theta_{\text{cr}} \simeq 1^\circ$  at  $\nu = 1$  GHz), and has a frequency-dependent width, inconsistent with the feeble RFM in the profile of J0631. Moreover, the CR beam is double, not quadruple.

## VII. SUMMARY AND DISCUSSION

Pulsar J0631+1036 appears to provide a very interesting instance in which the core/double cone model of ra-

radio pulsar emission geometry has difficulty providing an adequate description. The spectacular symmetric 4-peak of its profile at 1.4 GHz immediately suggests a double cone structure, but careful application of the model fails to give the ratio of conal emission radii derived for most pulsars, and it would suggest that the (putative) inner and outer cones are emitted at the same physical height. Such results have not been seen before in the pulsar population to which these ideas have been applied.

Under normal circumstances the apparent presence of a double cone would lead us to examine the pulsar’s physics in terms of the classic Ruderman & Sutherland (1975) polar cap model or its more recent modifications (*e.g.* Gil & Sendyk 2001). However, in the case of J0631+1036 we find that the required geometry (particularly the total absence of a core component at the centre of the profile) needs to be so contrived as to be implausible (see Section 5).

There are, of course, alternative physical models for pulsar emission. Petrova (2000), for example, has considered the effects of propagation phenomena on profile structure, but so far it seems that her approach does not provide much specificity and little information about polarization, although in some cases she does find configurations that produce four-component structures. Likewise, Beskin & Philippov (2011a,b) examine magnetospheric wave propagation, and the two concentric cones produced by their X- and O-mode beams seem a promising geometry to produce four-component profiles. However, they so far consider only orthogonal geometries, and the modal polarization of the model’s beam structure seems to disqualify the model for J0631+1036 whose highly polarized components appear to reflect only a single mode.

In this paper we have not attempted to rewrite the physics of pulsars, but suggest (§V) that J0631+1036 is a normal pulsar in an unusual environment. Noting that its magnetosphere is possibly enveloped by a dense star-formation region (Zepka *et al.* 1996), we speculate that some form of *downward* emission may contribute to the profile. After assessing various alternative component arrangements, in §V we suggest a simple model (Fig 8) consisting of a single narrow polar beam on either side of the pulsar which, combined with caustic effects, is able to account for the basic profile features, at least in geometric terms. The deep minimum at the centroid of the profile is then identified as the fiducial point (*i.e.* the instant at which the magnetic pole on the neutron star surface is directed towards us), which should be frequency-invariant.

This model has the drawback that it can only explain the observed polarisation by assuming that the entire profile adopts the polarisation of the leading nearside beam (perhaps in a manner suggested by Johnston & Weisberg 2006), and consciously ignores the unknown possible effects of the downflowing magnetospheric plasma on radio propagation. Furthermore, it fails to explain why the caustic effects it appeals to are not seen in other pulsars.

In an alternative approach (§6) we see the profile of J0631+1036 as arising from an intrinsically one-sided (wedge) beam located close to the pulsar surface. This would then categorise this pulsar among those found to have “missing” components on their trailing sides (Lyne & Manchester 1988, ET IX) and would thereby explain

why the PPA swing occurs so much later than the profile centroid. It has the obvious advantage of assuming all the radio emission is coming from the pulsar’s nearside, although the symmetrical fourfold structure of the wedge is an ad-hoc assumption that is difficult to justify physically. The observed subtle departures from profile symmetry are explained by the different sightline-cut geometry for different components (with no contribution from A/R effects). The deep minimum in the centre of the profile, the stumbling block for the classic double cone model, is now attributed to a physical separation of sectors within the emission wedge. However, in its geometric details, the model struggles to reconcile the observed PPA swing, profile width and component differences and may require a radical new look at emission processes (prompted by bifurcated emission components and the recent results of Desvignes *et al.* 2012).

A testable difference between the two types of model (twin beam vs. wedge) is the frequency alignment of the profiles. The twin beam will have an invariant fiducial point at the centroid of profile, whose width depends on a radius-to-frequency mapping (RFM). The wedge model claims little or no RFM occurs and attributes profile widening at lower frequencies to scattering. Simultaneous observations of the pulsar at widely-spaced frequencies could resolve this.

It is interesting to speculate about the nature of pulsar J0631+1036’s unusually large fractional linear polarization. In an OPM sense, its emission is nearly unimodal—that is, any secondary polarization-mode power must be at least roughly 10 times weaker across the profile than the primary mode power (except on the extreme edges of the outer component pair where some edge depolarization is seen). Following the Johnston & Weisberg (2006) reasoning, this suggests that the pulsar’s emission occurs above the polarization limiting height—that is, where the magnetospheric plasma is so tenuous that the normal propagation modes are essentially the same as those in vacuum. Here, the 600-km putative physical emission height corresponds to about 4% of the velocity-of-light cylinder radius, and the attenuation of the plasma may be responsible for fixing the same PPA swing for the entire profile, whatever the provenance of individual components.

While our attempts to model the J0631+1036 geometry have been confined entirely to the radio region, we note that great interest in the pulsar was generated following its detection in  $\gamma$  rays by Fermi LAT (Weltevrede *et al.* 2010). As in so many other such cases, the radio and  $\gamma$ -ray profiles could not be more different, the former being narrow and symmetrical and the latter broad and seemingly misaligned to the radio. Great effort, however, has recently been expended in understanding the beaming characteristics of pulsars in the  $\gamma$ -ray region. This discovery paper was able to argue that “ $\alpha$  was close to  $90^\circ$ ” and  $\beta \sim -4^\circ$ —but only, as the authors acknowledge, by assuming the entire profile is a single beam filling the open fieldlines. Seyffert *et al.* (2011) provide two models for the pulsar’s  $\gamma$ -ray emission region—the outer gap (OG) and two-pole caustic (TPC) models. In both models, the emission originates from gaps along the last open field lines, the difference being that, in the OG model,

emission originates above the null charge surface and interior to the last open field line, whereas the TPC gap is taken at the stellar surface. The OG model yields  $\alpha$  and  $\beta$  values of  $74\pm 5^\circ$  and  $-6\pm 2^\circ$ , respectively. The TPC model yields values of  $71\pm 6^\circ$  and  $-5\pm 3^\circ$ . Clearly these results are neither entirely incompatible nor obviously more accurate than our effort above. We see little basis for deciding between them, and we must accept that the mystery of J0631+1036 has yet to be resolved.

**Acknowledgments:** The authors thank the many colleagues who have responded to our challenge to consider the issues that pulsar J0631+1036 raises and have thus contributed to the discussions above. We also thank Dipanjan Mitra for adapting the RVM fitting software. GAEW thanks the University of Sussex for a Visiting Fellowship, and the Nederlandse Organisatie voor Wetenschappelijk Onderzoek (NWO) for a Visitor Bursary held at the “Anton Pannekoek” Astronomy Institute (API) of the University of Amsterdam. JMR also thanks the NWO for for a Visitor Grant and the API for their hospitality. Portions of this work were carried out with support from US National Science Foundation Grant AST 08-07691. Another part was supported by Polish National Science Centre grant DEC-2011/02/A/ST9/00256. Arecibo Observatory is operated by SRI International under a cooperative agreement with the National Science Foundation, and in alliance with Ana G. Mndez-Universidad Metropolitana, and the Universities Space Research Association. This work used NASA ADS system.

## REFERENCES

- Beskin, V. S. & Philippov, A. A. 2011a,b, arXiv1101.5733B & arXiv1107.3775B  
 Blaskiewicz, M., Cordes, J.M., Wasserman, I, 1991, *Ap.J.*, 370, 643  
 Desvignes, G., Kramer, M., Cognard, I., Kasian, L., van Leeuwen, J., Stairs, I., & Theureau G. 2012, Proc. IAU Symposium No. 291, ed. J. van Leeuwen, 199  
 Dyks, J., Rudak, B., & Harding, A. K. 2004, *Ap.J.*, 607, 939  
 Dyks J., & Rudak B., 2012, *MNRAS*, 420, 3403  
 Dyks, J., Frackowiak, M., Slowikowska, A., Rudak, B., & Zhang, B., 2005a, *Ap.J.*, 633, 1101  
 Dyks, J., Zhang, B., & Gil, J. 2005b, *Ap.J.*, 626, 45  
 Dyks, J., 2008, *MNRAS*, 607, 939  
 Dyks, J., Wright, G.A.E., Demorest, P., 2010a, *MNRAS*, 405, 509  
 Dyks, J., Rudak, B., & Demorest, P. 2010b, *MNRAS*, 401, 1781  
 Espinoza, C. M., Lyne, A. G., Stappers, B. W., & Kramer, M. 2011, *MNRAS*, 414, 1679  
 Everett, J.E. & Weisberg, J., 2001, *Ap.J.*, 553, 341  
 Force, M. M., & Rankin, J. M. 2010, *MNRAS*, 406, 237  
 Gangadhara R. T., & Gupta Y. 2001, *Ap.J.*, 555, 31  
 Guillemot, L., Kramer M., Johnson, T.J., Craig, H.A., Romani, R.W., Venter C., Harding, A.K., Ferdman, R.D., *et al.* 2013, *Ap.J.*, 768, 169  
 Jackson J.D., 1975, “Classical Electrodynamics”, John Wiley & Sons Inc, New York

- Johnston, S., & Weisberg, J. M. 2006, *MNRAS*, 368, 1856  
 Karastergiou, A. 2009, *MNRAS*, 392, 60  
 Kenena, J., *et al.* 2002, astro-ph/0202055  
 Malov, I. F., & Suleymanova, S.A. 1998, *Astron. Rep.*, 42, 388  
 McLaughlin, M. *et al.* 2004 in IAU Symp 218, Young Neutron Stars and their Environments, ed F. Camilo & B.M. Gaenschler (San Francisco: ASP)  
 Mitra, D., Rankin, J. M. 2010, *Ap.J.*, 727, 92 (ET IX)  
 Petrova, S. A., 2000, *A&A*, 360, 592.  
 Rankin, J. M. 2010, *Ap.J.*, 274, 333 (ET I)  
 Rankin, J.M. 1993, *Ap.J.*, 405, 285 and *A&A Suppl.*, 85, 145 (ET VI)  
 Romani R.W., & Yadigaroglu I.-A., 1995, *ApJ*, 438, 314  
 Seyffert, A. S., Venter, C., de Jager, O. C., Harding, A. K. 2011, arXiv:1105.4094v1  
 Srostlik, Z., & Rankin, J. M. 2005, *MNRAS*, 362, 1121  
 Thomas, R.M.C., Gupta, Y., & Gangadhara, R. T. 2010, *MNRAS*, 406, 1029  
 Weltevrede, P., Wright, G.A.E., Stappers, B., Rankin, J., 2006, *A&A*, 458, 269  
 Weltevrede, P., *et al.* 2010, *Ap.J.*, 708, 1426  
 Weltevrede P., Abdo A. A., Ackerman M., Ajello M., Axelsson M., Baldini, L., *et al.* 2010, *Ap.J.*, 708, 1426  
 Wright, G. A. E., 2003, *MNRAS*, 344, 1041  
 Zepka, A., Cordes, J. M., Wasserman, I., & Lundgren, S. C. 1996, *Ap.J.*, 456, 305